symmetry

MDPI

Article

Clustering of Floating Tracers in a Random Velocity Field Modulated by an Ellipsoidal Vortex Flow

Konstantin Koshel *, Dmitry Stepanov, Nata Kuznetsova and Evgeny Ryzhov

V.I.Il'ichev Pacific Oceanological Institute of FEB RAS, 43, Baltiyskaya St., 690041 Vladivostok, Russia; step-nov@poi.dvo.ru (D.S.); kuznetsova.nv@poi.dvo.ru (N.K.); ryzhovea@poi.dvo.ru (E.R.)
* Correspondence: kvkoshel@poi.dvo.ru; Tel.: +7-423-231-28-60

Abstract: The influence of a background vortex flow on the clustering of floating tracers is addressed. The vortex flow considered is induced by an ellipsoidal vortex evolving in a deformation. The system exhibits various vortex motion regimes: (1) a steady state, (2) oscillation and (3) rotation of the ellipsoidal vortex core. The latter two induce an unsteady velocity field for the tracer, thus leading to irregular (chaotic) tracer motion. Superimposing a stochastic divergent velocity field onto the deterministic vortex flow allows us to observe significantly different tracer evolution. An ellipsoidal vortex has ellipsoidal symmetry, and the tracer's trajectories exhibit the same symmetry inside the vortex. Outside the vortex, the external deformation flow symmetry dominates. Diffusion scattering and chaotic advection give tracers the opportunity to leave the region of ellipsoidal symmetry and form a picture of shear flow symmetry. We use the method of characteristics to integrate the floating tracer density evolution equation and the Euler Ito scheme for obtaining the floating tracer trajectories with a random velocity field. The cluster area and cluster mass from the statistical topography are used as the quantitative diagnostics of a floating tracer's clustering. For the case of a steady ellipsoidal vortex embedded into the deformation flow with a random velocity field component, we found that the clustering characteristics were weakened by the steady vortex. For the cases of an unsteady ellipsoidal vortex, we observed clustering in the floating tracer density field if the contribution of the divergent component was greater than or equal to that of the rotational (nondivergent) component. Even when the initial floating tracer patch was set on the boundary of the oscillating ellipsoidal vortex, we observed the formation of clusters. In the case of a rotating ellipsoidal vortex, we also observed pronounced clustering. Thus, we argue that unsteady ellipsoidal vortex regimes (oscillation and rotation), which induce chaotic motion of the nearby passive tracer's trajectories, are still conducive to clustering of floating tracers observed in the density field, despite the intense deformation introduced by strain and shear.

Keywords: tracer clustering; compressibility; ellipsoidal vortex; random flow

Citation: Koshel, K.; Stepanov, D.; Kuznetsova, N.; Ryzhov, E. Clustering of Floating Tracers in a Random Velocity Field Modulated by an Ellipsoidal Vortex Flow. *Symmetry* **2023**, *15*, 2211. https://doi.org/10.3390/sym15122211

Academic Editor: Rainer Hollerbach

Received: 7 November 2023
Revised: 13 December 2023
Accepted: 14 December 2023
Published: 18 December 2023

1. Introduction

Tracer evolution in various media often manifests significant heterogeneity of the tracer density or concentration fields even outside the tracer sources and sinks. In turbulent oceanic and atmospheric flows [1–3], this tracer aggregation is usually attributed to clustering (and its asymptotic version: exponential clustering). Under favorable conditions, tracers can be aggregated into coherent zones [4–6]. The area of these zones exponentially tends toward zero, and the dimensionless mass of the tracer tends toward unity. Many studies have established that ultimately, the velocity divergence is responsible for tracer clustering [3,7,8]. In addition, the importance of the horizontal shear of the velocity field, which can mediate the intensity of the tracer clustering, has been pointed out. However, these works addressed simplified stochastic models with limited applicability to more comprehensive models and natural experiments.

When looking at tracer aggregating induced by compressible velocity fields including oceanic flows, Jacobs et al. [3], Huntley et al. [7], Schumacher and Eckhardt [8], and Haza A.C. [9] have pointed out that mesoscale eddies trap tracer particles and significantly affect tracer aggregation. These studies used gridded velocity fields, which were the output from high-resolution ocean models. The gridded velocity fields were deterministic with non-vanishing divergence. However, the spatial resolution of the ocean models is limited by the grid scale, which means that all the sub-grid scales remained unresolved. One way to model these unresolved scales would be relying on superimposing random velocity components to the large-scale deterministic velocity field. The random component thus plays the role of small-scale dynamics.

Using this framework, where the velocity field consists of deterministic and random components, Stepanov et al. [10] studied the floating tracer aggregating and clustering embedded into the velocity field with a deterministic component from high-resolution model outputs. These studies confirmed that the shear flows associated with coherent vortex flows can significantly modulate floating tracer clustering. However, the deterministic component resulted from the interaction of many processes, and it was extremely complex to untangle all the involved processes and study them in detail. It did not allow one to determine the leading physical mechanisms driving floating tracer clustering.

The present study investigates the role of a background vortex flow in floating tracer clustering. The vortex flow is induced by an ellipsoidal vortex embedded into a deformation flow [11–13]. Using the model, where the velocity field consists of deterministic and random components, we focus on the influence of the ellipsoidal vortex motion on floating tracer clustering. Based on the diagnostics from the stochastic topography, we qualitatively estimate the clustering rate and clustering mass to confirm the importance of the vortex motion inducing chaotic behavior in the tracer trajectories for tracer clustering.

This paper is organized as follows. In Section 2, we formulate the general problem, the model of the random component, and the deterministic component model. Scaling of the equations and their integration are presented in Section 3. Section 4 considers the qualitative diagnostics for floating tracer clustering. The main results are in Section 5, followed by discussions in Section 6 and conclusions in Section 7.

2. Problem Formulation

The evolution of the passive tracer density $\rho(\mathbf{r}, t)$ under the rotational (nondivergent) velocity field $\mathbf{u}(\mathbf{r}, t) = (\mathbf{U}, w)(\mathbf{r}, t)$, where $\mathbf{U}$ and w are the horizontal and vertical velocity components, respectively, is governed by the following equations [14–16]:

$$\left(\frac{\partial}{\partial t} + \frac{\partial}{\partial \mathbf{r}}\mathbf{u}(\mathbf{r}, t)\right)\rho(\mathbf{r}, t) = \kappa\Delta\rho(\mathbf{r}, t) + Q, \;\; \rho(\mathbf{r}, 0) = \rho_0(\mathbf{r}), \tag{1}$$

where $\rho_0(\mathbf{r})$ is the initial density of the passive tracers, $\mathbf{r} = (\mathbf{R}, z) = (x, y, z)$ are the spatial coordinates, κ is the dynamic diffusivity, and Q is the source term. When $\kappa = 0$, $Q = 0$, and there is no tracer exchange across the region boundaries, then the random velocity field $\mathbf{u}(\mathbf{r}, t)$ with specified characteristics governs the stochastic features of Equation (1).

Let us consider the evolution of the floating tracer density $\rho(\mathbf{R}, z, t) = \rho(\mathbf{R}, t)\delta(z)$. Then, Equation (1) becomes

$$\left(\frac{\partial}{\partial t} + \frac{\partial}{\partial \mathbf{R}}\mathbf{U}(\mathbf{R}, t)\right)\rho(\mathbf{R}, t) = 0, \;\; \rho(\mathbf{R}, 0) = \rho_0(\mathbf{R}). \tag{2}$$

Here, the 2D velocity field $\mathbf{U}(\mathbf{R}, t)$ has potential (i.e., divergent) [4,14,17], and its divergence is governed by changes in w:

$$\nabla_{\mathbf{R}}\mathbf{U}(\mathbf{R}, t) = -\frac{\partial w(\mathbf{r}, t)}{\partial z}|_{z=0}, \tag{3}$$

where $\nabla_{\mathbf{R}}\mathbf{U}(\mathbf{R},t)$ is the horizontal divergence at the surface ($z=0$). When $w=0$, then $\mathbf{U}(\mathbf{R},t)$ is rotational (nondivergent).

We are interested in studying the influence of the deterministic nondivergent velocity field ($\mathbf{U}_e(\mathbf{R},t)$) on floating tracer clustering. Also, we assume that $\mathbf{U}_e(\mathbf{R},t)$ does not interact with the random velocity field ($\mathbf{U}_r(\mathbf{R},t)$). Therefore, the velocity field consists of two components:

$$\mathbf{U}(\mathbf{R},t)=\mathbf{U}_e(\mathbf{R},t)+\mathbf{U}_r(\mathbf{R},t). \tag{4}$$

2.1. Statistical Characteristics of the Random Velocity Field

As for our random velocity field, we consider a 2D velocity field with Gaussian, spatially homogeneous, isotropic, and stationary statistics [5]. We assume that the velocity field is δ correlated in time. This random velocity field consists of a divergent component ($\mathbf{U}_r^p(\mathbf{R},t)$) and a nondivergent component ($\mathbf{U}_r^s(\mathbf{R},t)$):

$$\mathbf{U}_r(\mathbf{R},t)=\gamma_r\mathbf{U}_r^p(\mathbf{R},t)+(1-\gamma_r)\mathbf{U}_r^s(\mathbf{R},t), \tag{5}$$

where γ_r is a contribution of the divergent component to the random velocity field. The associated spatiotemporal velocity correlation tensors are

$$B^j_{\alpha\beta}(\mathbf{R}',\eta)=\langle U^j_{r\alpha}(\mathbf{R},t)U^j_{r\beta}(\mathbf{R}+\mathbf{R}',t+\eta)\rangle=\int d\mathbf{k}E^j_{\alpha\beta}(\mathbf{k},\eta)e^{i\mathbf{k}\mathbf{R}'}, \tag{6}$$

where indices α and β stand for x and y, respectively, and indicate different components of the tensor. Index j stands for either p for divergent or s for nondivergent components. Then, we have

$$E^p_{\alpha\beta}(\mathbf{k},\eta)=E^p(k,\eta)\frac{k_\alpha k_\beta}{k^2},\ \ E^s_{\alpha\beta}(\mathbf{k},\eta)=E^s(k,\eta)\left(\delta_{\alpha\beta}-\frac{k_\alpha k_\beta}{k^2}\right). \tag{7}$$

Here, we use the spectral density in the form

$$E^p(k,\eta)=E^s(k,\eta)=\sigma^2_{\mathbf{U}}\frac{l^4}{4\pi}\exp\left\{-\frac{1}{2}k^2l^2\right\}\delta(\eta),$$

and l is the spatial correlation length.

We suppose that the spatiotemporal velocity correlation tensors satisfy the relations

$$B^j_{\alpha\beta}(\mathbf{0},0)=\langle U^j_{r\alpha}(\mathbf{R},t)U^j_{r\beta}(\mathbf{R},t)\rangle=\frac{1}{2}\sigma^2_{\mathbf{U}}\delta_{\alpha\beta}, \tag{8}$$

where $\sigma^2_{\mathbf{U}}=B^j_{\alpha\alpha}(\mathbf{0},0)=\int d\mathbf{k}E(k,0)$ for the nondivergent and divergent components of the random velocity field. The effective diffusivities corresponding to the divergent (D_p) and nondivergent (D_s) components of the random velocity field, respectively, are [4–6,18]

$$\begin{aligned} D_p&=\int_0^\infty d\eta\int d\mathbf{k}k^2E^p(k,\eta)=\int_0^\infty d\eta\left\langle\frac{\partial\mathbf{U}(\mathbf{R},t+\eta)}{\partial\mathbf{R}}\frac{\partial\mathbf{U}(\mathbf{R},t)}{\partial\mathbf{R}}\right\rangle,\\ D_s&=\int_0^\infty d\eta\int d\mathbf{k}k^2E^s(k,\eta)=\frac{1}{2}\int_0^\infty d\eta\langle\boldsymbol{\omega}(\mathbf{R},t+\eta)\boldsymbol{\omega}(\mathbf{R},t)\rangle, \end{aligned} \tag{9}$$

where $\boldsymbol{\omega}(\mathbf{R},t)=\boldsymbol{\nabla}\times(\mathbf{U}_r^s(\mathbf{R},t))$ is the velocity curl and $\frac{\partial\mathbf{U}_r^p(\mathbf{R},t)}{\partial\mathbf{R}}$ is the divergence of the random velocity field.

2.2. Velocity Field Induced by the Ellipsoidal Eddy

As for a deterministic velocity component, we consider a nondivergent 2D velocity field induced by an ellipsoidal vortex embedded in a deformation flow [11,13,19–21]. A detailed description of the ellipsoidal vortex model is presented in Appendix A. According to relations from the ellipsoidal vortex model (see Equation (A1) in the Appendix A for details), the velocity field components are determined by the solutions to the following system of equations:

$$\begin{aligned} \dot{a} &= ae\cos 2\theta, \quad \dot{b} = -be\cos 2\theta, \quad \dot{c} = 0, \\ \dot{\theta} &= -g\frac{\beta_0 b^2 - \alpha_0 a^2}{a^2 - b^2} + \gamma - e\frac{a^2+b^2}{a^2-b^2}\sin 2\theta, \\ \dot{x}_0 &= ex_0 - \chi y_0 + u_0, \quad \dot{y}_0 = \chi x_0 - ey_0 + v_0. \end{aligned} \tag{10}$$

Here a, b, and c are the semi-axes of the ellipsoidal vortex, and χ and e are the rotational and strain components of the deformation flow, respectively. Then, the velocity components $\mathbf{U}_e(u_e, v_e)$ satisfy the next relations:

$$\begin{aligned} u_e &= ex - \chi y + u_0 - \frac{\partial}{\partial y}\psi_v, \\ v_e &= \chi x - ey + v_0 + \frac{\partial}{\partial x}\psi_v, \end{aligned} \tag{11}$$

where ψ_v is the stream function associated with the ellipsoidal vortex (see Appendix A for details). Since the equations for the center of the ellipsoidal vortex are split, we can null them and suppose that $c(t) \equiv const$. Then, from the first two parts of Equation (10), we can obtain the relation $a(t)b(t) = const$. We denote $\varepsilon = \frac{b}{a}$, which features the relation between the semi-axes of the ellipsoidal vortex.

The system in Equations (10) and (11) for the trajectories of a passive tracer is a two-and-a-half-degree-of-freedom system, and thus the passive tracer trajectories can manifest chaotic behavior.

Koshel et al. [13] considered specific regimes of the ellipsoidal vortex motion and velocity field induced by these vortex motion regimes. This study considers these specific motions of the ellipsoidal vortex when ψ_v has a separatrix (the self-intersecting stream line), hyperbolic points, and the recirculation regions outside the ellipsoidal vortex [13]. Figure 1 shows a phase portrait of the ellipsoidal vortex motion regimes depending on ε and the angle θ.

Our deterministic velocity component is considered for three vortex motion regimes: (1) when the center of this vortex is fixed and (2) when the core of the ellipsoidal vortex oscillates or (3) rotates. In the first case, passive tracer trajectories coincide with the closed lines both within the vortex and outside it in the recirculation zones. In the second and third cases (see Figure 1c,d), passive tracer trajectories can manifest chaotic behavior in the recirculation zones and therefore influence the floating tracer clustering.

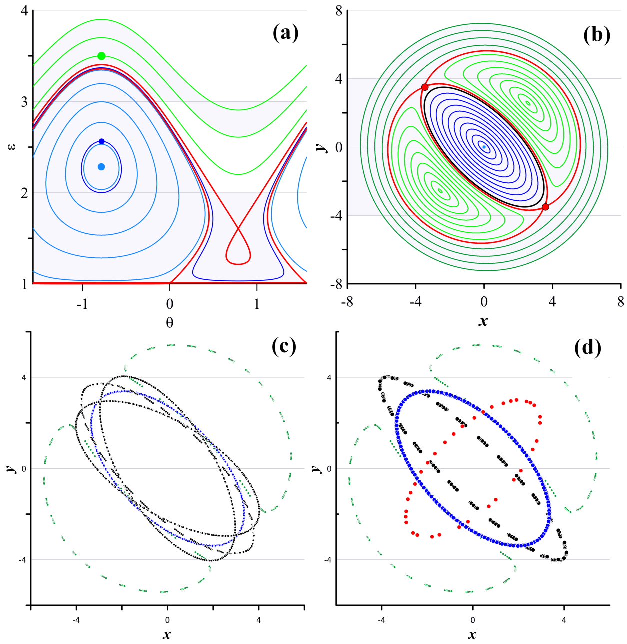

Figure 1. Motion regimes of the ellipsoidal vortex embedded in a deformation flow. (**a**) Phase portrait of the ellipsoidal vortex motion regimes (ε, θ). Various color points denote the initial states of the ellipsoidal vortex for three cases: the blue point ($\varepsilon = 2.28, \theta = -\pi/4$) denotes a steady state, when the vortex is stationary, the green point ($\varepsilon = 3.5, \theta = -\pi/4$) denotes an oscillation state, and the blue point ($\varepsilon = 2.56, \theta = -\pi/4$) denotes a case of the vortex's rotation. (**b**) Passive tracer trajectories inside the vortex (blue closed lines) and outside the vortex (green closed line) in a steady state. The red line denotes a separatrix, and the hyperbolic points are denoted by red points. (**c**) Positions of the vortex core boundary under oscillating of the ellipsoidal vortex. Blue points denote the initial state of the ellipsoidal vortex, and black points denote the positions of the vortex core boundary after 1/4, 1/2, and 3/4 of a period. Green points denote the position of the recirculation zone boundaries at the initial time moment. (**d**) Positions of the vortex core boundary for a rotating ellipsoidal vortex. Blue and green points denote the initial state of the ellipsoidal vortex and its recirculation zones, respectively. Red points denote the vortex core boundary after 1/4 and 3/4 of a period. Black points denote the vortex core boundary after 1/2 of a period.

3. Scaling of Floating Tracer Equations and Their Integration

We suppose that the variables of Equation (2) are dimensionless with spatial (L) and time (T) scales and a density scale (P). Since the random velocity field is δ-correlated in time, the scale T is equal to the time step. By having the spatial step equal to the time step, we can find the velocity scale $V = L/T$. The typical spatial scale of the ellipsoidal vortex or the b semi-axes is $L_{\text{vortex}} = 6 \times 10^2 \times L$, the typical rotation time of the vortex is $T_{\text{vortex}} = 2 \times 10^3 \times T$, the oscillation time of the vortex is $T_{\text{vortex}} = 2 \times 10^4 \times T$, and the typical time of diffusion scattering or the diffusion timescale is $2 \times 10^2 \times T$. For all numerical experiments, we used the next rms value $\sigma_{\text{U}} = 0.33$ and spatial correlation radius value $l = 8$.

For all of the following numerical experiments, we considered a square 2×2 patch as the initial condition. The patch was uniformly filled by 3.6×10^{10} floating markers. The initial patch was placed either within the vortex or on the boundary of the adjacent recirculation zone. The initial density of the floating tracer was always equal to unity.

To integrate Equation (2) given Equation (4), we used the method of characteristics [4,5]:

$$\frac{d\mathbf{R}}{dt} = \mathbf{U}(\mathbf{R}, t), \;\; \mathbf{R}(0) = \boldsymbol{\xi}, \\ \frac{d\rho}{dt} = -\frac{\partial \mathbf{U}(\mathbf{R}, t)}{\partial \mathbf{R}} \rho(t), \;\; \rho(0) = \rho_0(\boldsymbol{\xi}), \tag{12}$$

where $\boldsymbol{\xi}$ represents the initial coordinates of the floating marker. It is worth mentioning that we used many particles (characteristics), and due to clustering, we had many particles in the area of a high-density gradient.

In order to obtain the Eulerian density, the solution in Equation (12) needs to transform as follows:

$$\mathbf{R}(t) = \mathbf{R}(t; \boldsymbol{\xi}), \;\; \rho(t) = \rho(t; \boldsymbol{\xi}),$$

Then, to exclude ξ, we can obtain the density field

$$\rho(\mathbf{R}, t) = \rho(t) = \rho(t; \xi(\mathbf{R}; t)). \tag{13}$$

The system in Equation (12) of float tracer trajectories was integrated over time using the Euler Ito scheme [10,18]. We assumed that the random velocity components were constant in a sampling grid cell. Thus, we could solve Equation (12) analytically and estimate the time when the particle reached the boundary of the cell. Then, we used this solution as the initial condition in the next cell. We repeated this procedure until reaching the next time layer. This procedure allowed us to solve stochastic differential equations with undifferentiated coefficients. For example, the system in Equation (12) has the in-cell solution

$$\rho_{ijk} = \rho_{ijk-1} \exp\left\{ -\sum_{\tilde{k}=1}^{\tilde{n}} \frac{\partial \mathbf{U}\big(\tilde{i}, \tilde{j}, \tilde{k}\big)}{\partial \mathbf{R}} \Delta \tilde{t}_{\tilde{k}} \right\}.$$

Here, the indices with a tilde mark the cells through which the particle trajectory passes before reaching the next time layer, and $\Delta \tilde{t}_{\tilde{k}}$ represents the times before reaching the particle trajectory border of the next cell.

The method of the generation of the random velocity field is presented in [10,13,22]. We chose for the integration domain to be quite large to avoid the influence of the domain boundaries on the behavior of the floating tracer trajectories.

4. Qualitative Diagnostics of Floating Tracer Clustering

In order to qualitatively assess the impact of the deterministic component of the velocity field induced by the ellipsoidal vortex on the clustering, we used qualitative metrics or diagnostics from the statistical topography. The area was occupied by the clustered tracer or the clustering area ($\langle s_{\mathrm{hom}}(t; \bar{\rho})\rangle$) as well as the clustering mass ($\langle m_{\mathrm{hom}}(t; \bar{\rho})\rangle$). Let us consider the indicator of Liouville's function:

$$\varphi(\mathbf{R}, t; \bar{\rho}) = \delta(\rho(\mathbf{R}, t) - \bar{\rho}),$$

Then, the variable $S(t; \bar{\rho})$, where

$$S(t; \bar{\rho}) = \int d\mathbf{R}\theta(\rho(\mathbf{R}, t) - \bar{\rho}) = \int d\mathbf{R} \int_{\rho}^{\infty} d\rho' \varphi(\mathbf{R}, t; \rho'), \tag{14}$$

characterizes the total area of the regions, where the floating tracer density exceeding a predefined threshold $\bar{\rho}$, $\theta(\cdot)$ is the Heaviside (step) function, and the variable $M(t; \bar{\rho})$, where

$$M(t; \bar{\rho}) = \int d\mathbf{R}\rho(\mathbf{R}, t)\theta(\rho(\mathbf{R}, t) - \bar{\rho}) = \int d\mathbf{R} \int_{\rho}^{\infty} d\rho' \rho' \varphi(\mathbf{R}, t; \rho'), \tag{15}$$

is referred to as the cluster mass characterizing the mass of the floating tracers in these regions.

Ensemble averaging of $\varphi(\mathbf{R}, t; \bar{\rho})$ gives the single point in space and time probability density function $P(\mathbf{R}, t; \bar{\rho})$ [5,23]. Then, the averaging of Equations (14) and (15) on ensemble realizations of the random velocity field yields

$$\begin{aligned} \langle S(t;\bar{\rho})\rangle &= \int d\mathbf{R} \int_{\rho}^{\infty} d\rho' P(\mathbf{R}, t; \rho'), \\ \langle M(t;\bar{\rho})\rangle &= \int d\mathbf{R} \int_{\rho}^{\infty} d\rho' \rho' P(\mathbf{R}, t; \rho'). \end{aligned} \tag{16}$$

With the space and time homogeneous density field $\rho(\mathbf{R}, t)$, the single-point probability density function is independent from $\mathbf{R}$, and then Equation (16) is simplified as

$$\begin{aligned} \langle s_{\text{hom}}(t;\bar{\rho})\rangle = \langle \theta(\rho(\mathbf{R}, t) - \bar{\rho})\rangle = \mathrm{P}\{\rho(\mathbf{R}, t) > \bar{\rho}\} &= \int_{\rho}^{\infty} \mathrm{d}\rho' \mathrm{P}(t;\rho'), \\ \langle m_{\text{hom}}(t;\bar{\rho})\rangle &= \int_{\rho}^{\infty} d\rho' \rho' P(t;\rho'). \end{aligned} \tag{17}$$

Here, $s_{\text{hom}}(t;\bar{\rho})$ and $m_{\text{hom}}(t;\bar{\rho})$ are the specific cluster area and specific cluster mass, respectively [18].

For the random positive density field, the conditions for density clustering with the unity probability (that is, any realization of the random velocity field) yields the corresponding limits:

$$\langle s_{\text{hom}}(t;\bar{\rho})\rangle \to 0, \quad \langle m_{\text{hom}}(t;\bar{\rho})\rangle \to 1.$$

According to these relations, the area of the regions where the density exceeds the specified threshold $\bar{\rho}$ tends toward zero, and the mass concentrated into these regions (clusters) tends toward unity. When the evolution time is longer than the diffusion timescale, then we can use these estimates [5]:

$$\begin{aligned} \langle s_{\text{hom}}(t,\bar{\rho})\rangle = \mathrm{P}\{\rho(\mathbf{R}, t) > \bar{\rho}\} &\approx \sqrt{\frac{\rho_0}{\pi\bar{\rho}t/\tau}}\mathrm{e}^{-\frac{1}{4}\frac{t}{\tau}}, \\ \langle m_{\text{hom}}(t,\bar{\rho})\rangle/\rho_0 &\approx 1 - \sqrt{\frac{\bar{\rho}}{\pi\rho_0 t/\tau}}e^{-\frac{1}{4}\frac{t}{\tau}}. \end{aligned} \tag{18}$$

Here, $\tau = 1/D$, where D is the corresponding effective diffusivity, which is related to D_s and D_p as follows:

$$D_p = \gamma_r^2 D, \; D_s = (1-\gamma_r)^3 D.$$

Regardless, the $\langle s_{\text{hom}}(t;\bar{\rho})\rangle$ and $\langle m_{\text{hom}}(t;\bar{\rho})\rangle$ relations are valid only for the divergent component, and they can be useful diagnostics to quantitatively estimate the degree of floating tracer clustering.

According to the authors of [5], the effective diffusivity associated with the nondivergent component is modified when the random velocity field is modulated by the shear (γ) flow (Equation (A1)). In this case, the clustering process is absent. However, there is a filamentation which is associated with the diffusion scattering of the initial tracer patch [5], and the modified effective diffusivity ($D_{s\gamma}$) becomes

$$\begin{aligned} D_{s\gamma} &= D_s + \frac{2\gamma}{3D_s}, \quad (\gamma/D_s \ll 1); \\ D_{s\gamma} &= \sqrt[3]{\frac{3}{2}\gamma^2 D_s}, \quad (\gamma/D_s \gg 1), \end{aligned} \tag{19}$$

which shows that both under weak shear ($\gamma/D_s \ll 1$) and under strong shear ($\gamma/D_s \gg 1$), the random component dominates over the diffusion scattering.

5. Results

In this section, we present the results of our numerical experiments, where the clustering of floating tracers was simulated given the various states of the ellipsoidal vortex and the contributions of divergent and nondivergent components (Equation (4)).

First, let us consider the baseline experiment with no deterministic component (Equation (5)). Figure 2 shows the spatial distributions of the floating tracer density (Equation (13)) given various contributions of the divergent and nondivergent components. With only the divergent component, the tracer clustered into coherent regions (see Figure 2a). The floating tracer density reached 2×10^{36}. When the contribution of the divergent component decreased, and the contribution of the nondivergent component increased, we observed increasing patches with low values for the floating tracer density (see Figure 2b,c). In addition, due to the nondivergent component, the patches of the floating tracer with the highest density were scattered. With no divergent component, theoretical tracer clustering was prohibited (see Figure 2d), but some regions still demonstrated higher density values up to $\rho{\sim}10^2$.

These clustering features were confirmed by the quantitative diagnostics of the clustering (see Figure 2). The rate and degree of the floating tracer clustering were dependent on the contribution of the divergent component. The higher the contribution of the divergent component, the higher the rate of $\langle m_{\text{hom}}(t;\bar{\rho} > 1)\rangle$, and the lower the rate of $\langle s_{\text{hom}}(t;\bar{\rho} > 1)\rangle$. When the contribution of the divergent component was small or absent ($\gamma_r = 0.1/0.0$), the dependence of $\langle m_{\text{hom}}(t;\bar{\rho} > 1)\rangle$ differed from that of a high contribution from the divergent component. Given $\tau \gg D$, $\langle m_{\text{hom}}(t;\bar{\rho} > 1)\rangle$, when the contribution of the divergent component was not small ($\gamma_r = 1.0/0.5$), the clustering metrics continued to increase at a quite low rate. When $\gamma_r = 0.1/0.0$, in contrast, $\langle m_{\text{hom}}(t;\bar{\rho} > 1)\rangle$ decreased at a faster rate. This quantitatively reflects the decaying of the floating-tracer clustering when the contribution of the nondivergent component increased up until a complete absence of clusters when the nondivergent component dominated.

Let us consider now the cases where the velocity field consists of both a random component and deterministic component. The latter component was induced by the ellipsoidal vortex (Equation (4)). We considered a horizontal plane cutting the ellipsoid through the center. To start with, we considered the case of the steady ellipsoidal vortex. In this case, the deterministic component did not result in chaotic behavior for the tracer's trajectories (see Figure 2b)). Figure 3 shows the spatial distributions of the floating tracer density, depending on the contributions of the divergent component and the initial patch of floating tracers placed within the steady ellipsoidal vortex (see Figure 3a)). When the divergent component (Equation (4)) dominated, we observed regions with the highest values of the floating tracer density of up to 2×10^{36}. This confirms the theoretical exponential clustering of floating tracers. When the contribution of the divergent component decreased, the number of regions with the highest floating tracer density decreased as well, while the number of regions with low floating tracer densities increased. When the contribution of the nondivergent component increased, we observed diffusive scattering of the initial floating tracer patch, and the markers could leave the ellipsoidal vortex due to filamenting of the boundary of the floating tracer patch [5,22]. To illustrate these features of tracer trajectory behavior, the evolution of the floating tracer density was simulated during $\tau = Dt \gg 1$ for the case ($\gamma_r = 0.1/0.0$) (see Figure 3e,f). The initial floating tracer patch was scattering, and the floating tracer could leave the ellipsoidal vortex. Then, it could be advected by the background flow.

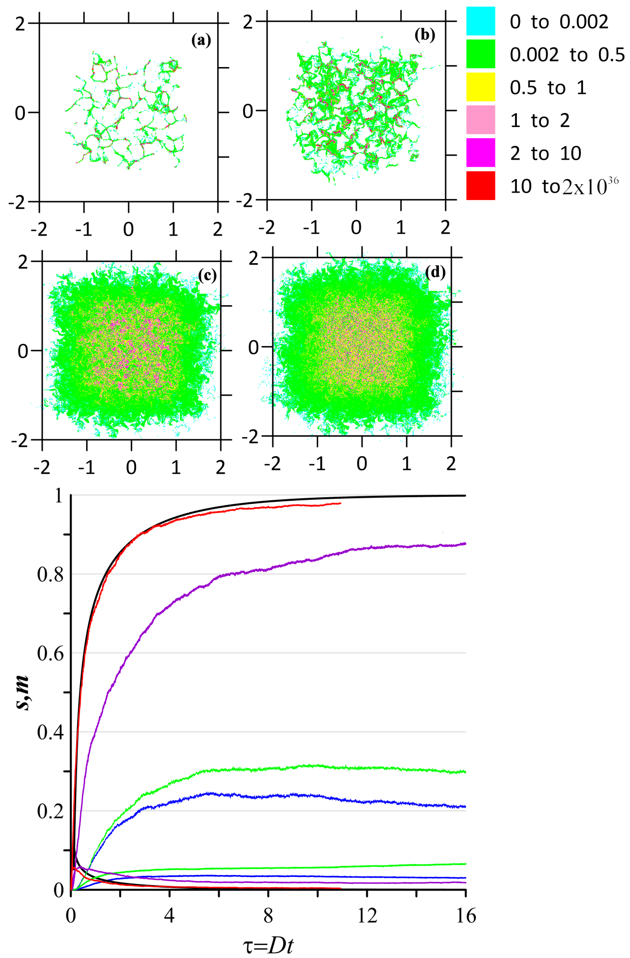

Figure 2. Baseline experiments, where floating tracer clustering was induced by the random velocity field only (Equation (5)). Instances of spatial distributions of the floating tracer density (Equation (13)) when (**a**) there was a divergent component only ($\gamma_r = 1.0$, $\tau = 10.94$), (**b**) contributions of the divergent and nondivergent components were equal ($\gamma_r = 0.5$, $\tau = 34.48$), (**c**) the contribution of the divergent component was small ($\gamma_r = 0.1$, $\tau = 34.48$), and (**d**) there was a nondivergent component only ($\gamma_r = 0.0$, $\tau = 34.48$). Colored lines at the bottom frame denote the evolution of the clustering areas $\langle s_{\text{hom}}(t;\bar{\rho} > 1)\rangle$ (lower curves) and the clustering mass $\langle m_{\text{hom}}(t;\bar{\rho} > 1)\rangle$ (upper curves), depending on various contributions of the divergent and nondivergent components. Red lines denote $\langle s_{\text{hom}}(t;\bar{\rho} > 1)\rangle$ and $\langle m_{\text{hom}}(t;\bar{\rho} > 1)\rangle$ curves, corresponding to the spatial distribution of the floating tracer density (see Figure 2a). Purple lines denote $\langle s_{\text{hom}}(t;\bar{\rho} > 1)\rangle$ and $\langle m_{\text{hom}}(t;\bar{\rho} > 1)\rangle$ curves, corresponding to the spatial distribution of the floating tracer density (see Figure 2b). Green lines denote $\langle s_{\text{hom}}(t;\bar{\rho} > 1)\rangle$ and $\langle m_{\text{hom}}(t;\bar{\rho} > 1)\rangle$ curves, corresponding to the spatial distribution of the floating tracer density (see Figure 2c). Blue lines denote $\langle s_{\text{hom}}(t;\bar{\rho} > 1)\rangle$ and $\langle m_{\text{hom}}(t;\bar{\rho} > 1)\rangle$ curves, corresponding to the spatial distribution of the floating tracer density (see Figure 2d). Finally, black lines denote $\langle s_{\text{hom}}(t;\bar{\rho} > 1)\rangle$ and $\langle m_{\text{hom}}(t;\bar{\rho} > 1)\rangle$ curves, corresponding to their analytical estimates (Equation (18)), when there was a divergent component only ($\gamma_r = 1.0$, $\tau = 10.94$) [17].

Qualitative diagnostics of the floating tracer clustering both for $\langle s_{\text{hom}}(t;\bar{\rho} > 1)\rangle$ and $\langle m_{\text{hom}}(t;\bar{\rho} > 1)\rangle$ confirmed the results (see Figure 3). The rate and degree of the clustering were higher when the contribution of the divergent component was high. We observed increasing of the clustering mass and decreasing of the clustering area. On the other hand, increasing of the contribution of the nondivergent component up to $\tau > 10$ led to a decrease in the floating tracer density within the ellipsoidal vortex. With time, we observed pronounced decreasing of the floating tracer density in the ellipsoidal vortex, and $\langle m_{\text{hom}}(t;\bar{\rho} > 1)\rangle$ decreased.

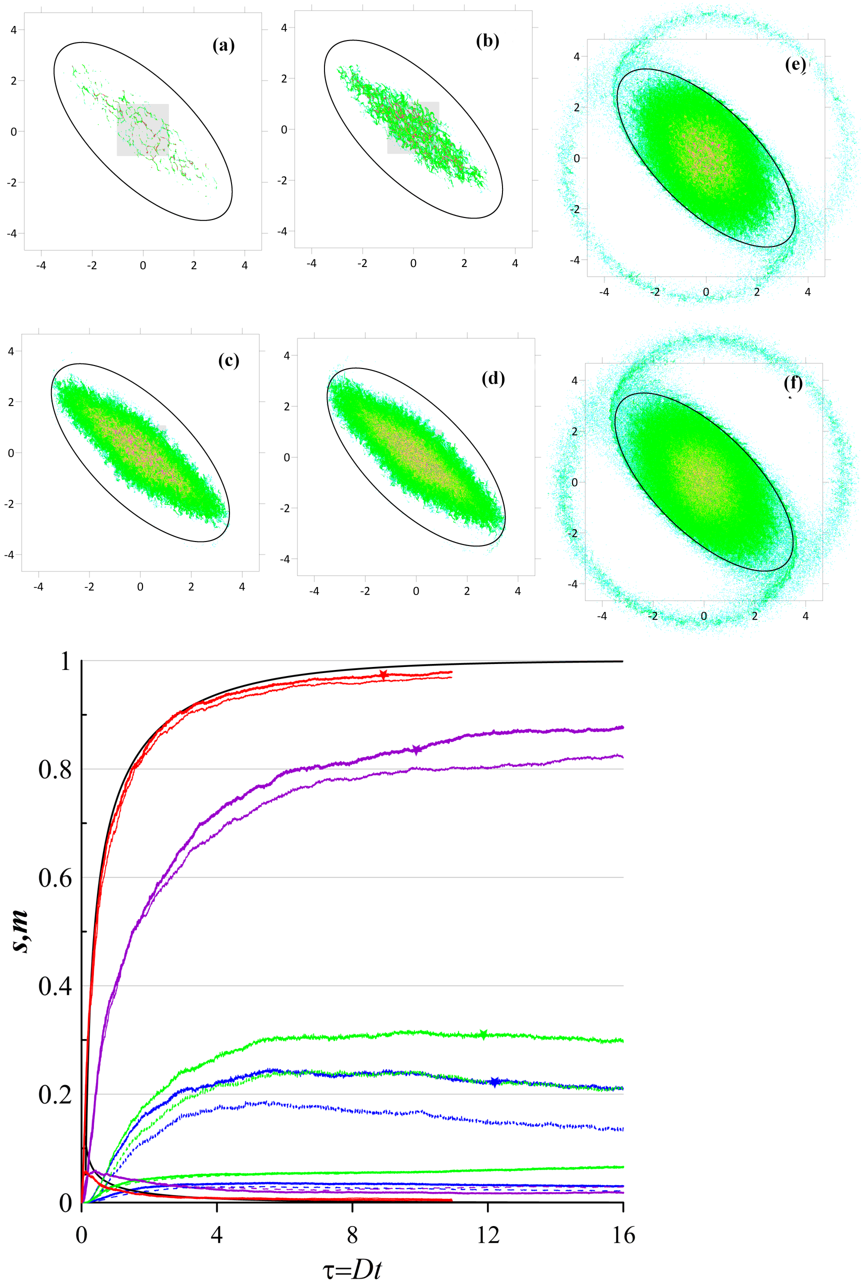

Figure 3. The same as Figure 2, but with the deterministic velocity component (Equation (4)) induced by a steady ellipsoidal vortex. Frames (**a**–**d**) corresponds the same valies of γ_r end τ as in Figure 2. For cases (**c**,**d**), see the insets (**e**,**f**), respectively, at the time $\tau = 94.44$. Colored lines denote the clustering area $\langle s_{\text{hom}}(t;\bar{\rho} > 1)\rangle$ (lower curves) and the clustering mass $\langle m_{\text{hom}}(t;\bar{\rho} > 1)\rangle$ (upper curves) given various contributions from the divergent and nondivergent components. Curves of $\langle m_{\text{hom}}(t;\bar{\rho} > 1)\rangle$ for the random velocity field only(Equation (5)) are denoted by the colored asterisks.

Figure 4 shows the spatial distribution of the floating tracer density for the case where the floating tracer patch was initially located near the boundary of the steady ellipsoidal vortex (see Figure 4a). In this case, the floating tracer clustering was observed because of the contribution of the divergent component. Note that the floating tracers were clustering near both the boundary of the ellipsoidal vortex and the boundary of the recirculation regions. When the nondivergent component increased, we observed strong diffusive scattering of the tracer (see Figure 4c,d). At the same time, anisotropy of the spatial distribution of the floating tracer was manifested. High density values were observed mainly near the boundary of the vortex and recirculation zones, while the markers did not penetrate deep into the vortex or centers of the recirculation zones.

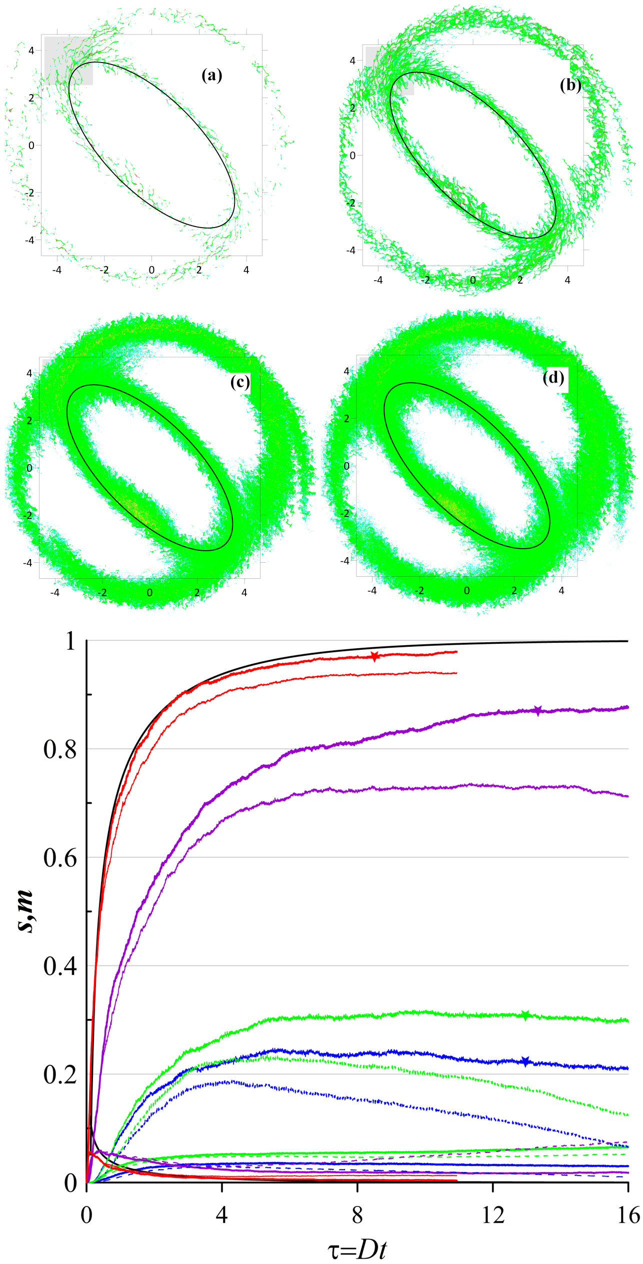

Figure 4. The same as Figure 3, but the initial tracer patch was placed near the boundary of the steady ellipsoidal vortex.

Quantitative diagnostics pointed out that the floating tracer clustered exponentially when there was no nondivergent component (see Figure 4). At earlier times, a sharp increase in the clustering mass was observed, and the $\langle m_{\rm hom}(t;\bar{\rho} > 1)\rangle$ metric was non-decreasing. For the non-asymptotic cases, when the contribution of the nondivergent component was neither zero nor unity, and at a longer characteristic time $\tau \gg 1$, we observed a significant decrease in $\langle m_{\rm hom}(t;\bar{\rho} > 1)\rangle$, and thus the clusters did not fully form. Note that the rate of decay depends on the contribution of the nondivergent component.

Let us consider the clustering of the floating tracer with the deterministic component induced by the oscillating and rotating ellipsoidal vortex regimes (see Figure 2c,d). Koshel et al. [13] established that for both cases, the tracer trajectories can manifest chaotic behavior. To start with, we considered the case of the oscillating vortex regime and placed an initial tracer patch within the vortex or within the recirculation zone's boundary.

Figure 5 shows the spatial distributions of the tracer density when the initial patch was placed within the vortex. According to these distributions, the higher the contribution of the divergent component, the more the tracer was clustered. Note that the initial tracer patch was scattered along the semi-axes of the ellipsoidal vortex.

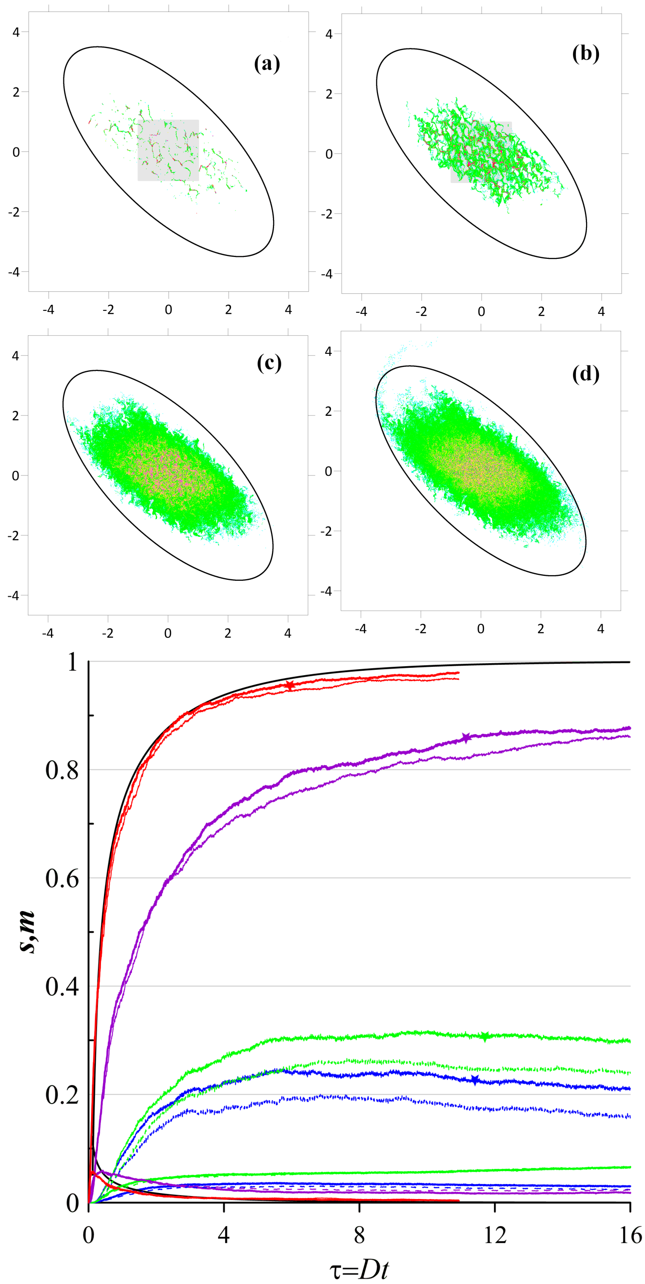

Figure 5. The same as Figure 3, but for the oscillating ellipsoidal vortex regime.

Quantitative diagnostics of the tracer clustering confirmed that the highest values of the cumulative clustered mass w along with extremely small values for the cumulative clustered area were observed when the contribution of the divergent component was quite high (see Figure 5). At the same time, when the contribution of the divergent component was minimal with time $\tau \gg 1$, we observed little clustering. This process of no clustering can also be seen in the curve for $\langle m_{\text{hom}}(t; \bar{\rho} > 1) \rangle$.

Figure 6 shows the spatial distributions of the tracer density when the initial tracer patch was placed near the oscillating ellipsoidal vortex's boundary. With a dominant divergent component, the tracer clustering manifested itself prominently. The clusters were generated mainly near the boundaries of the vortex and recirculation zones. The clusters were, however, not generated deeper within the vortex core or the centers of the recirculation zones. Increasing the contribution of the nondivergent component resulted in diffusive scattering of the tracer and weakened clustering with spatial heterogeneity.

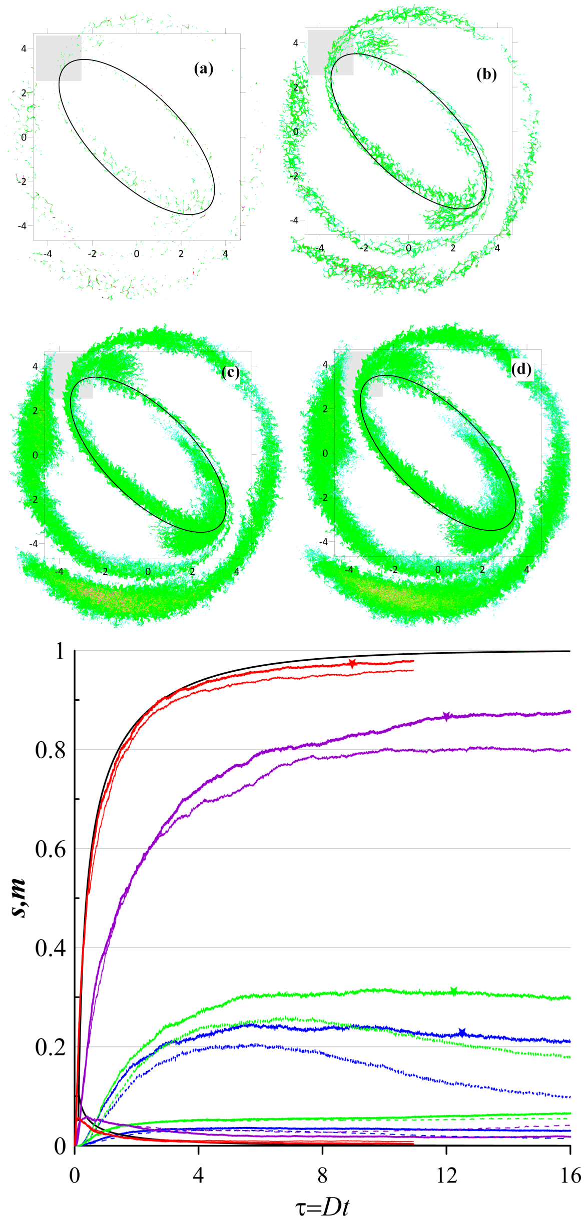

Figure 6. The same as Figure 5, but the initial tracer patch was placed near the boundary of the oscillating ellipsoidal vortex.

Quantitative diagnostics of the clustering showed that again, when the divergent component dominated, the clustering happened at higher rates (see Figure 6). As time moved on, the $\tau \gg 1$, $\langle m_{\text{hom}}(t; \bar{\rho} > 1) \rangle$ curve continued its non-decreasing behavior. When the contribution of the divergent component decreased, the clustering again was not able to be sustained. This was confirmed by the $\langle m_{\text{hom}}(t; \bar{\rho} > 1) \rangle$ curve for larger times $\tau \gg 1$ (see Figure 6).

To finalize this section, we considered clustering of the tracer in the rotating ellipsoidal vortex regime. Figure 7 shows the spatial distributions of the tracer density when the initial tracer patch was placed within the ellipsoidal vortex core. Clustering of the tracer was similarly governed by the contribution of the divergent component. Reducing this contribution led to a smaller probability of clustering. At the same time, increasing the contribution of the nondivergent component facilitated diffusive scattering of the tracer. However, even when the nondivergent component was dominant, there were still many zones of nonzero values for the tracer density within the ellipsoidal vortex.

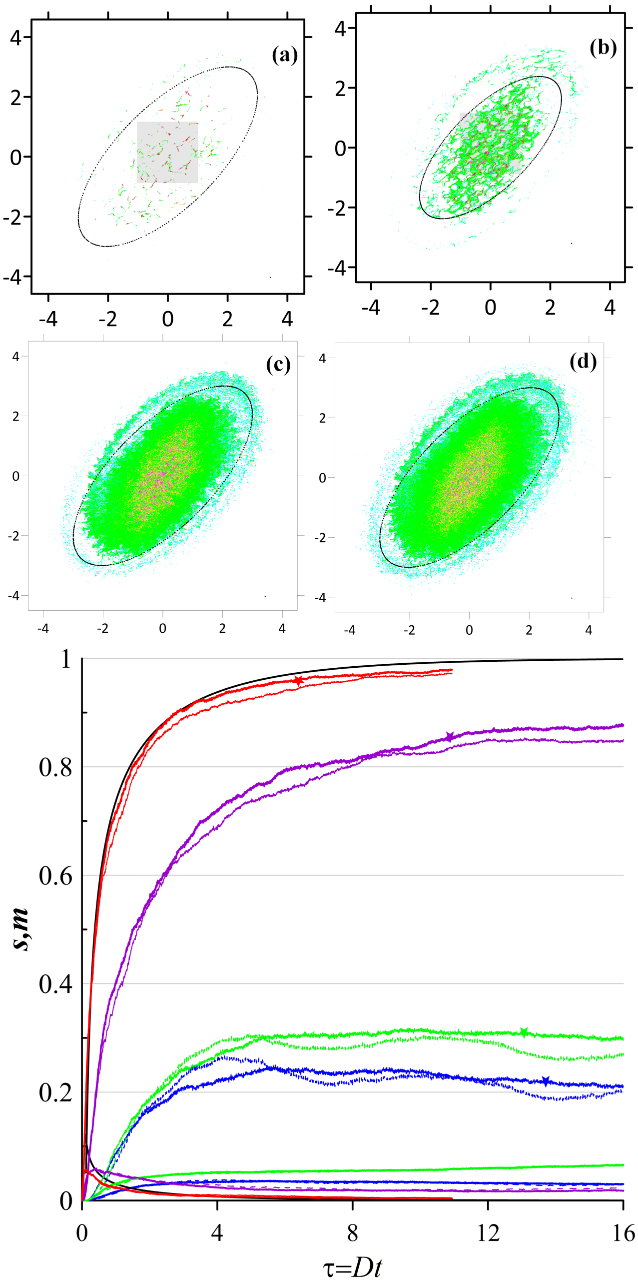

Figure 7. The same as Figure 3 but for the rotating ellipsoidal vortex.

According to the diagnostics of the clustering, we observed a high clustering rate and then non-decreasing behavior from the clustering mass for the case when the contributions of the random velocity component were equal to the deterministic one ($\gamma_r = 0.5$) (see Figure 7). Note that if the divergent component was small, and at longer times $\tau \gg 1$, the $\langle m_{\text{hom}}(t; \bar{\rho} > 1) \rangle$ curve still showed no decreasing behavior, but it oscillated with the period of τ 6 dimensionless units of time. When the contribution of the divergent component was equal to zero, the sharp clustering rate during the initial period changed to a slow decrease in the clustering degree at $\tau \gg 1$, similar to the previously described case with a period of τ 6 dimensionless units of time.

Finally, let us consider the case where the initial tracer patch was placed near the boundary of the rotating ellipsoidal vortex (see Figure 8). The spatial distributions of the tracer density show that clustering occurred near the boundaries of the vortex and recirculation zones similarly because of the large divergent component. When the contribution of the divergent component decreased, the zones with the highest density values became less pronounced. On the other hand, with increasing the nondivergent component, we observed more pronounced diffusive scattering (see Figure 8c,d). When there was only the nondivergent component, there were still multiple tracer aggregations in the recirculation zones and partially in the vortex itself, but the density was rather small (see Figure 8d).

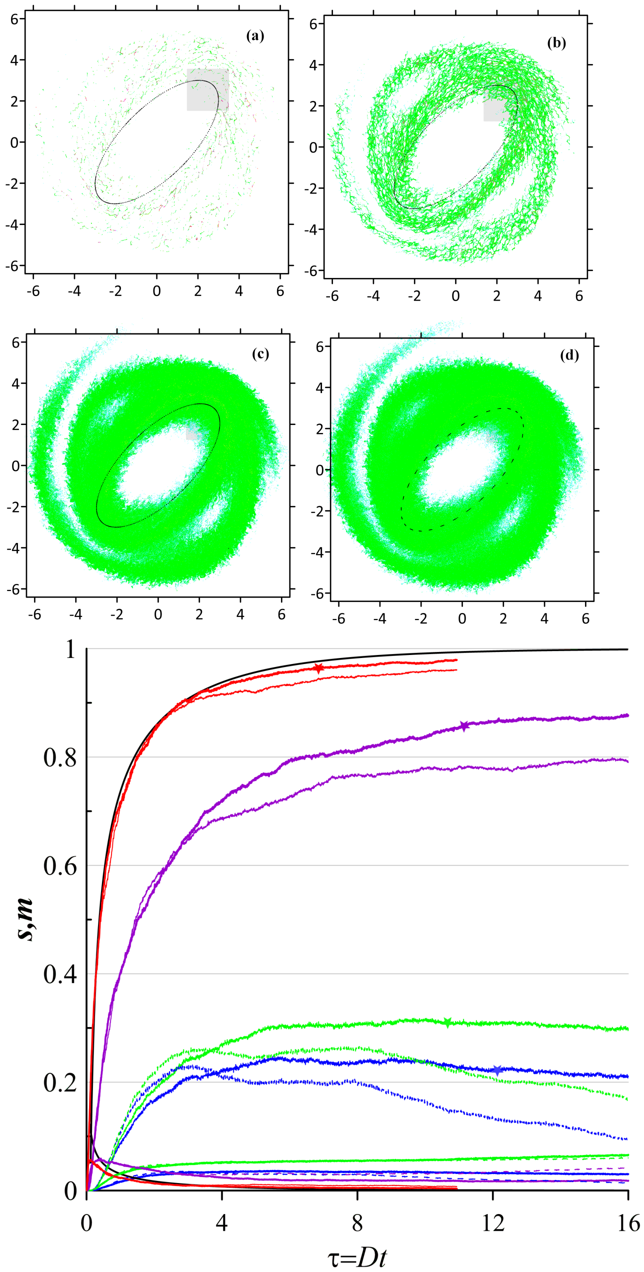

Figure 8. The same as Figure 7, but the initial tracer patch was placed near the boundary of the rotating ellipsoidal vortex.

Quantitative diagnostics of the clustering confirmed clustering with a dominant divergent velocity component (see Figure 8). When $\gamma_r = 1$ or $\gamma_r = 0.5$, clustering became weaker. However, the $\langle m_{\text{hom}}(t; \bar{\rho} > 1)\rangle$ curve did not manifest decreasing behavior with longer times $\tau \gg 1$. On the other hand, increasing the contribution of the nondivergent component resulted in a slow increase in the tracer mass and consequently in the decrease in the $\langle m_{\text{hom}}(t; \bar{\rho} > 1)\rangle$ curve with longer times $\tau \gg 1$. Similarly, the larger contribution of the nondivergent component, the more the cluster mass decreased.

6. Discussion

One of the aims of this investigation was to consider the results from [10,18] in more detail by employing a simpler dynamical model of the background shearing flow. The authors studied the floating tracer clustering in a compound velocity field, where the random velocity component consisted of divergent and nondivergent parts and the deterministic velocity component was taken from a gridded velocity field from eddy-resolving numerical simulations of the Sea of Japan circulation. Various regimes of tracer aggregation were reported and analyzed. However, due to the complexity of the comprehensive ocean velocity field, a detailed analysis of the leading processes responsible for the observed dynamical patterns was not fully addressed. The authors suggest that the observed features associated with the qualitative diagnostics of the tracer clustering were mostly affected by multiple eddies populating the deterministic velocity field. In the present study, we considered a simpler model of a vortex, namely the velocity field induced by an ellipsoidal vortex embedded into a deformation flow. In particular, we focused on the influence of the ellipsoidal vortex motion regimes (oscillating and rotating) on the tracer clustering.

When comparing the clustering metrics depending on the balance parameter γ_r for the steady ellipsoidal vortex case, it is shown that the clustering occurred only with a dominant divergent velocity component. When γ_r was equal to 0.5, the floating tracer clustered within the vortex. In other cases, clustering did not occur. Even though the clustering mass increased initially (up to $\tau = 8Dt$), then it started decreasing ($\tau \gg Dt$), as evidenced by the $\langle m_{\text{hom}}(t; \bar{\rho} > 1)\rangle$ curve. Compared with the baseline purely stochastic model, this suggests that the presence of a steady ellipsoidal vortex is not conducive to tracer clustering. This was most noticeable when the γ_r ratio was quite small.

In addition, tracer clustering is sensitive to the tracer's initial conditions. When the initial tracer patch was placed near the ellipsoidal vortex periphery, clustering was weakened, as opposed to the case where the initial tracer patch was placed within the vortex. This is because the recirculation zones near the separatrix experience the most intense shearing flows. At early times ($\tau \ll 10Dt$), the clustering rate in the steady state vortex case was similar to the baseline purely stochastic case. At later times ($\tau \gg Dt$), the difference between these two cases increased, and the clustered mass in the steady state vortex case was less than that in the baseline case.

When considering the case of an oscillating ellipsoidal vortex, we observed significant changes. For two different sets of initial tracer conditions, the tracer clustering occurred for both a dominant divergent velocity component ($\gamma_r = 1.0$) and for equal contributions of the divergent and nondivergent components ($\gamma_r = 0.5$). This was confirmed by the non-decreasing $\langle m_{\text{hom}}(t; \bar{\rho} > 1)\rangle$ curves for these two sets of initial conditions. When increasing the influence of the nondivergent component ($\gamma_r \ll 0.5$), the tracer clustering never happened (the $\langle m_{\text{hom}}(t; \bar{\rho} > 1)\rangle$ curves attenuated in both cases with the initial conditions).

A noticeably different case was the rotating ellipsoidal vortex. With a dominant divergent velocity component or equal contributions from both velocity components, the clustering rate was higher when compared with all the previous cases. Also, the clustering process differed for the two sets of the tracer's initial conditions. When the initial tracer patch was placed within the rotating vortex, the clustering was stronger compared with the case where the initial tracer patch was placed near the periphery of the recirculation zones. We also observed a high clustering rate with a dominating nondivergent component ($\gamma_r \ll 1.0$).

We thus demonstrated pronounced differences between the tracer clustering occurring in the steady ellipsoidal vortex regime and in the oscillating or rotating ellipsoidal vortex regimes. When the ellipsoidal vortex was unsteady, the tracer trajectories manifested chaotic behavior, which partly accounted for the differences. When the initial tracer patch was placed within the ellipsoidal vortex, the clustering mass for the case of an unsteady vortex was higher than that for the case of a steady ellipsoidal vortex.

Thus, we confirmed the hypothesis from [10] that clusters cannot survive strong advection near eddies for long. When an ellipsoidal vortex is steady, the tracer is advected from the vortex rather slowly. However, the tracer is also trapped in the neighborhood of the separatrix for a long time. This region has strong shearing flows that prevent clustering.

When the ellipsoidal vortex is unsteady, the tracer is advected from the neighborhood of the separatrix (where the strongest shearing flows are observed, which are detrimental for clustering), which allows a larger part of the mass to remain clustered. This is observed for the case of the initial tracer patch placed near the periphery of the ellipsoidal vortex. In this case, due to the unsteady ellipsoidal vortex and tracer advection, the tracer leaves the neighborhood of the separatrix away from strong shears. This prevents decreasing of the clustering rate in contrast to the steady ellipsoidal vortex case.

7. Conclusions

This study investigated the influence of a background vortex flow on the clustering of floating tracers. The vortex flow was induced by the interaction of an ellipsoidal vortex with a deformation flow, which produces various vortex motion regimes: (1) steady state, (2) oscillating, and (3) rotating of the ellipsoidal vortex. The unsteady ellipsoidal vortex induced chaotic tracer trajectories. The regions where the chaotic behavior largely manifested itself were hyperbolic points and separatrix. We focused on tracer clustering in velocity fields where the deterministic velocity component permitted chaotic tracer trajectories.

The tracer clustering was governed by a random velocity field consisting of nondivergent and divergent components. With a dominant divergent component, we observed tracer clustering. On the other hand, with a dominant nondivergent component, the clustering never occurred.

The spatial and time scales of the vortex motion exceeded those of the random velocity field by an order of magnitude. For the deterministic velocity component induced by the ellipsoidal vortex, the random velocity component therefore was mostly independent. We used the method of characteristics to integrate the tracer density equation and the Euler Ito scheme for tracer trajectories evolving in the random velocity field. The clustering area and clustering mass from the statistical topography were used as the quantitative diagnostics of the tracer clustering.

In the baseline case of a random velocity field only, we confirmed that when the divergent component dominated, there were zones with a rather small total area and quite high mass in the tracer density field. According to the quantitative metrics, the cumulative mass of these zones was non-decreasing with time. When the contribution of the divergent component relative to the nondivergent component was less than 0.5, we registered no tracer clustering.

For the steady ellipsoidal vortex regime, we observed weaker tracer clustering. Even with a higher contribution from the divergent component, the clustering rate and clustering degree were not as strong compared with the baseline case. The most striking differences were observed for the initial tracer patch placed near the boundary of the ellipsoidal vortex. We also observed complete floating tracer clustering when the random velocity field consisted of the divergent component only.

For the unsteady ellipsoidal vortex regimes, we observed tracer clustering when the contribution of the divergent component was higher than or equal to that of the nondivergent component. Even when the initial tracer patch was placed near the boundary of the recirculation zones, clustering still persisted. With a rotating ellipsoidal vortex, we observed pronounced clustering as well. When the initial tracer patch was placed within the rotating vortex, the clustering rate was higher than that for the baseline case during earlier times. Thus, we suggested that the unsteady ellipsoidal vortex regimes promoted (or at least did not prohibit) clustering due advecting the nascent clusters away from the separatrix region, where the strongest shears existed.

Author Contributions: Conceptualization, K.K.; methodology, K.K.; software, K.K. and N.K.; validation, K.K., E.R. and D.S.; formal analysis, K.K.; investigation, K.K.; resources, K.K.; data curation, K.K.; writing—original draft preparation, K.K. and D.S.; writing—review and editing, D.S. and E.R.; visualization, K.K. and N.K.; supervision, K.K.; project administration, K.K.; funding acquisition, K.K. All authors have read and agreed to the published version of the manuscript.

Funding: This study was supported by the Russian Science Foundation, grant no. 23-27-00188 (https://rscf.ru/en/project/23-27-00188/).

Data Availability Statement: For more specific information about the simulated data, email Konstantin Koshel at kvkoshel@poi.dvo.ru.

Conflicts of Interest: The authors declare no conflicts of interest. The funders had no role in the design of the study; in the collection, analyses, or interpretation of data; in the writing of the manuscript; or in the decision to publish the results.

Appendix A. Ellipsoidal Vortex in the Deformation Flow

According to [11,13,19–21], let us consider the deformation flow in the dimensionless coordinates

$$\mathbf{u}_e = (ex - \gamma y, \gamma x - ey) \tag{A1}$$

where e and γ are dimensionless variables controlling the time scale and $\mathbf{u}_e = (u, v)$ is a dimensionless variable controlling the velocity scale.

We consider a vortex structure embedded in a deformation flow (Equation (A1)), and the vortex is an ellipsoidal region V with the boundary

$$F(x, y, z, t) = \frac{\tilde{x}^2}{a^2(t)} + \frac{\tilde{y}^2}{b^2(t)} + \frac{\tilde{z}^2}{c^2(t)} = 1, \tag{A2}$$

where

$$\begin{gathered} \tilde{x} = (x - x_0)\cos\theta(t) + (y - y_0)\sin\theta(t), \\ \tilde{y} = -(x - x_0)\sin\theta(t) + (y - y_0)\cos\theta(t), \\ \tilde{z} = \eta, \end{gathered} \tag{A3}$$

and $x_0(t), y_0(t), z_0 = 0$ is the vortex's center and $c(t) = BN\bar{c}(t)$, where $\bar{c}(t)$ is the semi-axes. The vorticity is considered piecewise constant. There is a difference between the vorticity inside the vortex and adjacent flow

$$q = \begin{cases} 2\gamma, & \mathbf{r} \notin V, \\ 2\alpha, & \mathbf{r} \in V, \end{cases} \tag{A4}$$

According to [13], the stream function is $\psi = \psi_e + \psi_v$, where $\psi_e = (x^2 + y^2)\gamma/2 - exy - u_0 y + v_0 x$. Thus, ψ_e and ψ_v satisfy the relations

$$\Delta\psi_e = 2\gamma; \quad \Delta\psi_v = \begin{cases} 0, & \mathbf{r} \notin V, \\ 2(\alpha - \gamma) = g, & \mathbf{r} \in V. \end{cases} \tag{A5}$$

For ψ_v, we have the following solutions[11,19–21]:

$$\psi_v(x,y,z,t) = -\frac{gabc}{2}\int_{\lambda}^{\infty}(1 - \frac{\tilde{x}^2}{a^2+\mu} - \frac{\tilde{y}^2}{b^2+\mu} - \frac{\tilde{z}^2}{c^2+\mu})\frac{d\mu}{\sqrt{\tilde{\Delta}(\mu)}}. \tag{A6}$$

Here, $z = \tilde{z} = \eta$, $\tilde{\Delta}(\mu) = (a^2+\mu)(b^2+\mu)(c^2+\mu)$. The lower limit of the integration $\lambda(\tilde{x},\tilde{y},\tilde{z},t)$ is defined as the root of the cubic equation

$$\frac{\tilde{x}^2}{a^2+\lambda} + \frac{\tilde{y}^2}{b^2+\lambda} + \frac{\tilde{z}^2}{c^2+\lambda} = 1.$$

We take $\lambda = 0$ to be inside the ellipsoidal vortex and $\lambda > 0$ to be outside the vortex. The fluid particle advection equations are

$$\begin{aligned} \frac{dx}{dt} &= u = ex - \gamma y + u_0 - \frac{\partial}{\partial y}\psi_v, \\ \frac{dy}{dt} &= v = \gamma x - ey + v_0 + \frac{\partial}{\partial x}\psi_v. \end{aligned} \tag{A7}$$

According to [11,19–21], from the kinematic conditions, we take the relations for the parameters and positions of the ellipsoid to be

$$\begin{aligned} \dot{a} = ae\cos 2\theta, \quad \dot{b} &= -be\cos 2\theta, \quad \dot{c} = 0, \\ \dot{\theta} = -g\frac{\beta_0 b^2 - \alpha_0 a^2}{a^2 - b^2} &+ \gamma - e\frac{a^2+b^2}{a^2-b^2}\sin 2\theta, \\ \dot{x}_0 = ex_0 - \gamma y_0 + u_0, &\quad \dot{y}_0 = \gamma x_0 - ey_0 + v_0, \end{aligned} \tag{A8}$$

where

$$\alpha_0 = abc\int_0^{\infty}\frac{1}{a^2+\mu}\frac{d\mu}{\sqrt{\tilde{\Delta}(\mu)}}, \quad \beta_0 = abc\int_0^{\infty}\frac{1}{b^2+\mu}\frac{d\mu}{\sqrt{\tilde{\Delta}(\mu)}}, \quad \chi_0 = abc\int_0^{\infty}\frac{d\mu}{\sqrt{\tilde{\Delta}(\mu)}}. \tag{A9}$$

The spatial derivatives of the stream function can be obtained by introducing new coordinates as follows:

$$\begin{aligned} \frac{\partial}{\partial \tilde{x}}\psi_v &= \tilde{x}gabc\int_{\lambda}^{\infty}\frac{1}{a^2+\mu}\frac{d\mu}{\sqrt{\tilde{\Delta}(\mu)}}, \\ \frac{\partial}{\partial \tilde{y}}\psi_v &= \tilde{y}gabc\int_{\lambda}^{\infty}\frac{1}{b^2+\mu}\frac{d\mu}{\sqrt{\tilde{\Delta}(\mu)}}, \end{aligned} \tag{A10}$$

which are the velocity projections onto the main semi-axes of the ellipsoid. Taking into account Equation (A3), we obtain

$$\begin{aligned} \frac{\partial}{\partial x}\psi_v &= \cos\theta\frac{\partial}{\partial \tilde{x}}\psi_v - \sin\theta\frac{\partial}{\partial \tilde{y}}\psi_v, \\ -\frac{\partial}{\partial y}\psi_v &= -\sin\theta\frac{\partial}{\partial \tilde{x}}\psi_v - \cos\theta\frac{\partial}{\partial \tilde{y}}\psi_v. \end{aligned} \tag{A11}$$

References

1. Okubo, A. Diffusion and Ecological Problems: Mathematical Models. In *Biomathematics*; Springer: Berlin/Heidelberg, Germany, 1980; Volume 10.
2. McComb, W.D. *The Physics of Fluid Turbulence*; Oxford Engineering Science Series; Clarendon Press: Oxford, UK, 1990; Volume 25.

3. Jacobs, J.A.; Huntley, H.S.; Kirwan, A.D.; Lipphardt, B.L.; Campbell, T.; Smith, T.; Edwards, K.; Bartes, B. Ocean processes underlying surface clustering. *J. Geophys. Res. Ocean.* **2016**, *121*, 180–197. [CrossRef]
4. Klyatskin, V.I. The imbedding method in statistical boundary-value wave problems. In *Book Series: Progress in Optics*; Elsevier: Amsterdam, The Netherlands, 1994; Volume 33, pp. 1–133. [CrossRef]
5. Klyatskin, V.I. *Stochastic Equations: Theory and Applications in Acoustics, Hydrodynamics, Magnetohydrodynamics, and Radiophysics*; Springer: Berlin/Heidelberg, Germany, 2015; Volume 1–2.
6. Klyatskin, V.I. Stochastic structure formation in random media. *Phys. Usp.* **2016**, *59*, 67–95. [CrossRef]
7. Huntley, H.S.; Lipphardt, B.L.; Jacobs, G.; Kirwan, A.D. Clusters, deformation, and dilation: Diagnostics for material accumulation regions. *J. Geophys. Res. Ocean.* **2015**, *120*, 6622–6636. [CrossRef]
8. Schumacher, J.; Eckhardt, B. Clustering dynamics of Lagrangian tracers in free-surface flows. *Physcal Rev. E* **2002**, *66*, 017303. [CrossRef] [PubMed]
9. Haza A. C., Özgökmen, T.M.H.P. Impact of submesoscales on surface material distribution in a gulf of Mexico mesoscale eddy. *Ocean. Model.* **2016**, *107*, 28–47. [CrossRef]
10. Stepanov, D.V.; Ryzhov, E.A.; Zagumennov, A.A.; Berloff, P.; Koshel, K.V. Clustering of Floating Tracer Due to Mesoscale Vortex and Submesoscale Fields. *Geophys. Res. Lett.* **2020**, *47*, e2019GL086504. [CrossRef]
11. Zhmur, V.V. Localized eddy formation in a shear-flow. *Oceanology* **1988**, *28*, 536–538.
12. Meacham, S.P.; Pankratov, K.K.; Shchepetkin, A.F.; Zhmur, V.V. The interaction of ellipsoidal vortices with background shear flows in a stratified fluid. *Dyn. Atmos. Oceans* **1994**, *21*, 167–212. [CrossRef]
13. Koshel, K.V.; Ryzhov, E.A.; Carton, X.J. Vortex Interactions Subjected to Deformation Flows: A Review. *Fluids* **2019**, *4*, 14. [CrossRef]
14. Klyatskin, V.I. Clustering and diffusion of particles and passive tracer density in random hydrodynamic flows. *Phys. Uspekhi* **2003**, *46*, 667–688. [CrossRef]
15. Klyatskin, V.I. Diffusion and clustering of sedimenting tracers in random hydrodynamic flows. *J. Exp. Theor. Phys.* **2004**, *99*, 1005–1017. [CrossRef]
16. Cressman, J.R.; Goldburg, W.I. Compressible Flow: Turbulence at the Surface. *J. Stat. Phys.* **2003**, *113*, 875. [CrossRef]
17. Klyatskin, V.I.; Saichev, A.I. Statistical theory of the diffusion of a passive tracer in a random velocity field. *J. Exp. Theor. Phys.* **1997**, *84*, 716–724. [CrossRef]
18. Koshel, K.V.; Stepanov, D.V.; Ryzhov, E.A.; Berloff, P.; Klyatskin, V.I. Clustering of floating tracers in weakly divergent velocity fields. *Phys. Rev. E* **2019**, *100*, 063108. [CrossRef]
19. Zhmur, V.V. Subsurface mesoscale eddy structures in a stratificated ocean. *Oceanology* **1989**, *29*, 28–32.
20. Zhmur, V.V.; Pankratov, K.K. The dynamics of the semi-ellipsoid subsurface vortex in the non-uniform flow. *Oceanology* **1989**, *29*, 205–211.
21. Zhmur, V.V.; Pankratov, K.K. Dynamics of mesoscale eddy formation in the field currents of large intensive vortex. *Okeanologia* **1990**, *30*, 124–129.
22. Klyatskin, V.I. Statistical description of the diffusion of a passive tracer in a random velocity field. *Phys. Uspekhi* **1994**, *37*, 501–513. [CrossRef]
23. Isichenko, M. Percolation, statistical topography, and transport in random media. *Rev. Mod. Phys.* **1992**, *64*, 961. [CrossRef]